Available online at www.sciencedirect.com
SCIENCE DIRECT®
Journal of Power Sources 134 (2004) 262–276
JOURNAL OF POWER SOURCES
www.elsevier.com/locate/jpowsour

Extended Kalman filtering for battery management systems of LiPB-based HEV battery packs Part 2. Modeling and identification

Gregory L. Plett*,[1]

Department of Electrical and Computer Engineering, University of Colorado at Colorado Springs, 1420 Austin Bluffs Parkway, P.O. Box 7150, Colorado Springs, CO 80933-7150, USA

Received 27 January 2004; accepted 26 February 2004

Available online 28 May 2004

Abstract

Battery management systems in hybrid electric vehicle battery packs must estimate values descriptive of the pack's present operating condition. These include: battery state of charge, power fade, capacity fade, and instantaneous available power. The estimation mechanism must adapt to changing cell characteristics as cells age and therefore provide accurate estimates over the lifetime of the pack.

In a series of three papers, we propose a method, based on extended Kalman filtering (EKF), that is able to accomplish these goals on a lithium ion polymer battery pack. We expect that it will also work well on other battery chemistries. These papers cover the required mathematical background, cell modeling and system identification requirements, and the final solution, together with results.

In order to use EKF to estimate the desired quantities, we first require a mathematical model that can accurately capture the dynamics of a cell. In this paper we "evolve" a suitable model from one that is very primitive to one that is more advanced and works well in practice. The final model includes terms that describe the dynamic contributions due to open-circuit voltage, ohmic loss, polarization time constants, electro-chemical hysteresis, and the effects of temperature. We also give a means, based on EKF, whereby the constant model parameters may be determined from cell test data. Results are presented that demonstrate it is possible to achieve root-mean-squared modeling error smaller than the level of quantization error expected in an implementation.

Keywords: Battery management system (BMS); Hybrid electric vehicle (HEV); Extended Kalman filter (EKF); State of charge (SOC); State of health (SOH); Lithium-ion polymer battery (LiPB)

1. Introduction

This paper is the second in a series of three that describe advanced algorithms for a battery management system (BMS) for hybrid electric vehicle (HEV) application. This BMS is able to estimate battery state of charge (SOC), power fade, capacity fade and instantaneous available power, and is able to adapt to changing cell characteristics over time as the cells in the battery pack age. The algorithms have been implemented on a lithium-ion polymer battery (LiPB) pack, but we expect them to work well for other battery chemistries.

The method that we use to estimate these parameters is based on Kalman filter theory. (There have been other reported methods for SOC estimation that use Kalman filtering [1,2], but the method in this series of papers expands on these results and also differs in some important respects, as will be outlined later.) Kalman filters are an intelligent—and sometimes optimal—means for estimating the state of a dynamic system. By modeling our battery system to include the wanted unknown quantities in the "state", we may use the Kalman filter to estimate their values. An additional benefit of the Kalman filter is that it automatically provides dynamic error-bounds on these estimates as well. We exploit this fact to give aggressive performance from our battery pack, without fear of causing damage by overcharge or overdischarge.

* Tel.: +1-719-262-3468; fax: +1-719-262-3589.
E-mail addresses: glp@eas.uccs.edu, gplett@compactpower.com (G.L. Plett).
URL: http://mocha-java.uccs.edu.
[1] The author is also consultant to Compact Power Inc., Monument, CO 80132, USA. Tel.: +1-719-488-1600; fax: +1-719-487-9485.

0378-7753/$ – see front matter © 2004 Elsevier B.V. All rights reserved.
doi:10.1016/j.jpowsour.2004.02.032

The first paper [3] is an introduction to the problem. It describes the HEV environment and the requirement specifications for a BMS. The remainder of the paper is a brief tutorial on the Kalman filter theory necessary to grasp the content of the remaining papers; additionally, a nonlinear extension called the "extended Kalman filter" (EKF) is discussed.

This second paper describes some mathematical cell models that may be used with this method. The HEV application is a very harsh environment, with rate requirements up to and exceeding $\pm 20C$ and very dynamic rate profiles. This is in contrast to relatively benign portable-electronic applications with constant power output and fractional C rates. Methods for estimating SOC that work well in portable-electronic devices may not work well in the HEV application. If precise SOC estimation is required by the HEV, then a very accurate cell model is necessary.

Results of lab tests on physical cells are presented and compared with model prediction. The best modeling results obtained to date are so precise that the root-mean-squared (RMS) estimation error is less than the quantization noise floor expected in our battery management system design. More importantly, the model allows very precise SOC estimation, therefore allowing the vehicle controller to confidently use the battery pack's full operating range without fear of over- or under-charging cells. This paper also gives an overview of other modeling methods in the literature and shows how an EKF may be used to adaptively identify unknown parameters in a cell model, in real time, given test data.

The third paper [4] covers the real-time parameter estimation problem; namely, how to dynamically estimate SOC, power fade, capacity fade, available power and so forth. An EKF is used in conjunction with the cell model. The cell model may be fixed, or may itself have adaptable parameters so that the model tracks cell aging effects. Details for a practical implementation are discussed.

We now proceed by briefly reviewing cell models in the literature that have been proposed for SOC estimation. We explain why these do not meet the requirements presented in [3]. Several models from Refs. [5,6] do meet the requirements, and they are described in detail here, together with some new models and results. A method for identifying model parameters using an extended Kalman filter is presented, followed by conclusions.

2. Standard cell-modeling methods for SOC estimation

The literature documents a number of cell-modeling methods for SOC estimation. An excellent summary, in greater detail than can be presented here, may be found in reference [7]. Here, we investigate to see whether any of these methods meets our needs. Recall that our application is to model cell dynamics for the purpose of SOC estimation in an HEV battery pack.

For this application, the cell model must be accurate for all operating conditions. These include: very high rates (up to about $\pm 20C$, far exceeding the low rates considered by many papers in the literature for portable electronic applications), temperature variation in the automotive range of -30 to $50\,^{\circ}\mathrm{C}$, very dynamic rates (unlike the more benign portable electronic and battery electric vehicle application). Charging must be accounted for in the model.

We also require non-invasive methods using only readily available signals. This requirement is imposed by the HEV environment where the BMS has no direct control over current and voltage experienced by the battery pack—these are in the domain of the vehicle controller and inverter. We must rely on such measurements as instantaneous cell terminal voltage, cell current and cell external temperature.

Our cell chemistry also limits the range of approaches we might consider. Techniques specific to lead-acid chemistries, for example, are not appropriate for LiPB cells.

2.1. Laboratory and chemistry-dependent methods

Several methods for direct SOC estimation simply cannot be used in our application:

1. A laboratory method for determining SOC is to completely discharge a cell, recording discharged ampere-hours, to determine its present remaining capacity. This is the most accurate SOC measurement technique, but is impractical in HEV as the battery energy is wasted by the test, and the test cannot dynamically estimate SOC.
2. Chemistry-dependent methods for other chemistries, such as Coup de Fouet measurement, or measurement of electrolyte physical properties for lead-acid batteries, are all inappropriate (as our application uses LiPB cells).
3. Open-circuit voltage (OCV) measurements: If the cell is allowed to rest for a long period, its terminal voltage decays to OCV, and OCV may be used to infer SOC (via lookup table, for example). However, long periods (sometimes hours) of battery inactivity must occur before the terminal voltage approaches OCV. This method may not be used for dynamic SOC estimation. (Other complications with this method include the dependence of OCV on temperature, and presence of terminal voltage hysteresis, especially at low temperatures.)

2.2. Electro-chemical modeling

One approach to modeling cell electrical dynamics is to carefully consider, at the molecular level, the various processes that occur within the cell. Accurate terminal voltage prediction may be achieved by these models (see Ref. [8], for example). However, it would be difficult (if possible) to measure the many required physical parameters on a cell-by-cell basis in a high-volume consumer product. We have not pursued this approach, although

we employ many of the macroscopic concepts in our models.

2.3. Impedance spectroscopy

Another broad category of cell modeling involves measuring cell impedances over a wide range of ac frequencies at different states of charge [9–13]. Values of the model parameters are found by least-squares fitting to measured impedance values. SOC may be indirectly inferred by measuring present cell impedance and correlating them with known impedances at various SOC levels. We must also discount this method for our application, as we have no direct method to inject signals into cells to measure impedances. We rely on the vehicle to generate and dissipate all energy flowing through the battery pack.

2.4. Circuit models

A number of papers present equivalent circuit models of cells [14–17]. Typically, a high-valued capacitor or voltage source is used to represent the open-circuit voltage. The remainder of the circuit models the cell's internal resistance and more dynamic effects such as terminal voltage relaxation. From the OCV estimate, SOC may be inferred via table lookup. Both linear- and nonlinear-circuit models may be used. Our model has many similarities to a circuit model, except that our fundamental "state" is SOC, not OCV.

2.5. Coulomb counting

The final method discussed in the literature involves SOC estimation directly via Coulomb counting. This may be done "open-loop", which is very sensitive to current measurement error, or "closed-loop" which can be much more accurate. The feedback mechanism may be empirically designed [18] or may use a mathematically optimized approach such as the Kalman filtering method [1,2] to generate the feedback. All Kalman filtering-based methods by other authors in the literature (with which we are familiar) use a circuit model of the cell with voltage sources and capacitor voltages representing OCV and relaxation effects. OCV may be estimated and SOC inferred from OCV.

Our approach is also based on the Kalman filtering method, but the fundamental aspect of our model that sets it apart from those reported in the literature is that SOC itself is required to be a state of the system. The direct benefit of this approach is that the Kalman filter automatically gives a dynamic estimate of the SOC and its uncertainty (this is discussed in greater detail in Ref. [4]). That is, instead of reporting the SOC to the vehicle controller (at some point in time) to be "about 55%", the algorithm is able to report that the SOC is $55 \pm 3\%$, for example. This allows the vehicle controller to confidently use the battery pack's full operating range without fear of over- or under-charging cells.

3. An evolution of cell model structures

In order to use Kalman-based methods for a battery management system, we must first have a cell model in a discrete-time state-space form. Specifically, we assume the form

$$x_{k+1} = f(x_k, u_k) + w_k, \tag{1}$$

$$y_k = g(x_k, u_k) + v_k, \tag{2}$$

where x_k is the system state vector at discrete-time index k, where the "state" of a system comprises in summary form the total effect of past inputs on the system operation so that the present output may be predicted solely as a function of the state and present input. Values of past inputs are not required. The vector u_k is the measured exogenous system input at time k and w_k is unmeasured "process noise" that affects the system state. The system output is y_k and v_k is measurement noise, which does not affect the system state. Equation (1) is called the "state equation", (2) is called the "output equation", and $f(\cdot,\cdot)$ and $g(\cdot,\cdot)$ are (possibly nonlinear) functions, specified by the particular cell model used. All of the system dynamics are represented in (1). Equation (2) is a static relationship. In the models to follow, w_k is used to account for current-sensor error and inaccuracy of the state equation, and v_k is used to account for voltage sensor error and inaccuracy of the output equation.

In the case where we wish to model a cell's dynamics using (1) and (2), the vector u_k contains the instantaneous cell current i_k. It may also contain the cell temperature T_k, an estimate of the cell's capacity C, and/or an estimate of the cell's internal resistance R_k, for example. The system output is typically a scalar but may be vector valued as well. Here we consider the output to be the cell's loaded terminal voltage (not its at-rest OCV). Our method constrains the state vector x_k to include SOC as one component.

There are many possible candidates for (1) and (2), and for the choice of x_k and u_k. Here, we describe the development of some modeling equations in an evolutionary sense. That is, we start with a very simple model, and gradually add complexity to better represent the true cell dynamics. In order to justify the changes in the model, we compare model dynamics to cell dynamics based on data collected from cell tests. We first describe the cell tests, and then develop the model structures.

3.1. Cell tests for model fitting

In order to compare the abilities of the proposed models to capture a cell's dynamics, we gathered data from a prototype LiPB cell. The cell comprises a $LiMn_2O_4$ cathode, an artificial graphite anode, is designed for high-power applications, has a nominal capacity of 7.5 Ah and a nominal voltage of 3.8 V. For the tests, we used a Tenney thermal chamber set at 25°C and an Arbin BT2000 cell cycler. Each channel of the Arbin was capable of 20 A current, and ten channels were

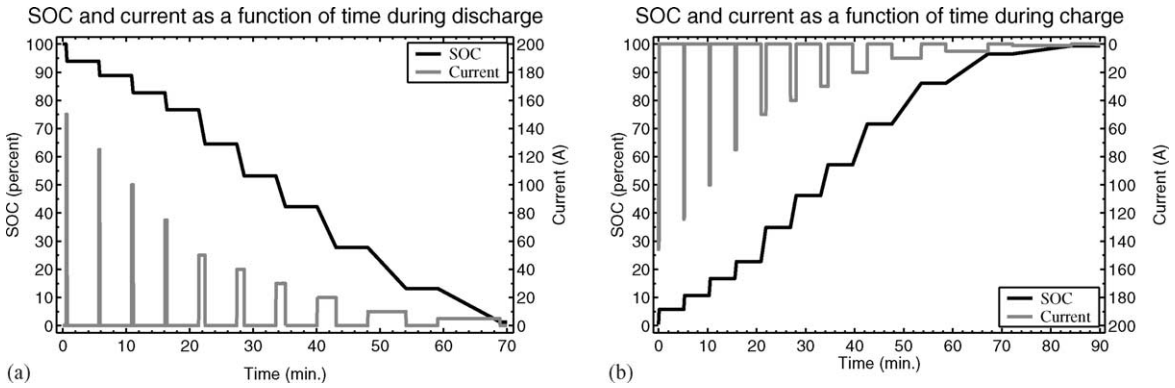

Fig. 1. Plots showing SOC vs. time and rate vs. time for pulsed-current cell tests. Discharge portion of test is shown in (a); charge portion of test is shown in (b). Dark line is SOC, gray line is current.

connected in parallel to achieve currents of up to 200 A. The cycler's voltage measurement accuracy was ±5 mV and its current measurement accuracy was ±200 mA.

Two types of cell tests were performed for the work reported in this paper. The first type comprised a sequence of constant-current discharge pulses and rests followed by a sequence of constant-current charge pulses and rests. The cell started fully charged before the test began. Discharge current pulses from 150 down to 1 A, and charge pulses from 150 down to 1 A were used. The current and SOC profiles for this test are shown in Fig. 1(a) and (b). Frame (a) shows the discharge portion of the test and frame (b) shows the charge portion of the test. Data points (including voltage, current, ampere-hours discharged and ampere-hours charged) were collected once per second.

The second test was a sequence of 16 urban dynamometer driving schedule (UDDS) cycles, separated by 40 A discharge pulses and 5 min rests, and spread over the 90–10% SOC range. The SOC as a function of time is plotted in Fig. 2(a), and rate as a function of time for one of the UDDS cycles is plotted in Fig. 2(b). We see that SOC increases by about 5% during each UDDS cycle, but is brought down about 10% during each discharge between cycles. The entire operating range for these cells (10–90% SOC) is excited during the cell test.

The data was used to identify parameters of the cell models to be described in the next sections. The goal is to have the cell model output resemble the cell terminal voltage under load as closely as possible, at all times, when the cell model input is equal to the cell current. Model fit was judged by comparing root-mean-squared estimation error (estimation error equals cell voltage minus model voltage) over the portions of the cell tests where SOC was between 5 and 95%. Model error outside that SOC range was not considered as the HEV pack operation design limits are 10–90% SOC.

3.2. SOC as a state-vector component

The one constant requirement for the cell model is that we constrain SOC, denoted as z_k, to be a member of the state vector x_k. To be careful, we give a list of definitions culminating in our understood definition of SOC.

- *Definition*: A cell is *fully charged* when its voltage reaches $v = v_h$ after being charged at infinitesimal current levels. Here, we use $v_h = 4.2$ V at room temperature (25 °C).
- *Definition*: A cell is *fully discharged* when its voltage reaches $v = v_l$ after being drained at infinitesimal current levels. Here, we use $v_l = 3.0$ V at room temperature.

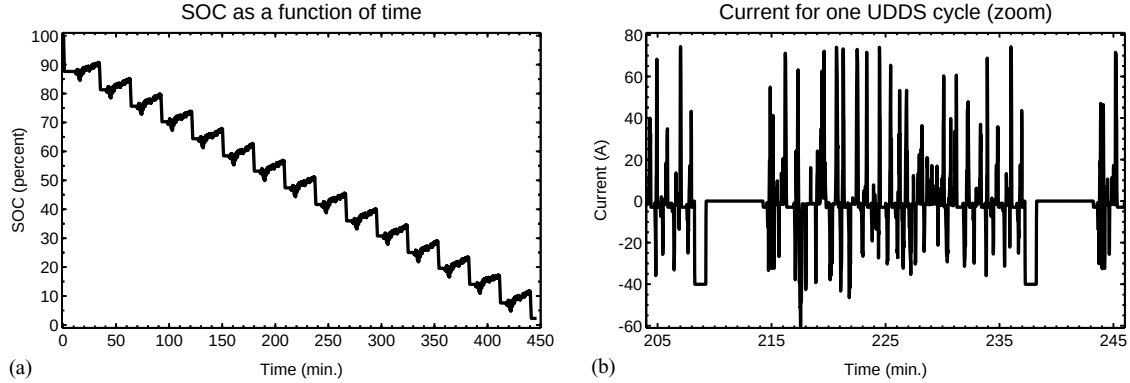

Fig. 2. Plots showing SOC vs. time and rate vs. time for UDDS cell tests. SOC is shown in (a); rate for one UDDS cycle is shown in (b).

- *Definition*: The *capacity* of a cell C is the maximum number of ampere-hours that can be drawn from the cell before it is fully discharged, at room temperature, starting with the cell fully charged.
- *Definition*: The *nominal capacity* C_n of the cell is the number of ampere-hours that can be drawn from the cell at room temperature at the $C/30$ rate, starting with the cell fully charged.
- *Definition*: The SOC of the cell is the ratio of the remaining capacity to the nominal capacity of the cell, where the remaining capacity is the number of ampere-hours that can be drawn from the cell at room temperature at the $C/30$ rate before it is fully discharged.

With these definitions in place, we can then investigate some mathematical relations involving SOC. Particularly,

$$z(t) = z(0) - \int_0^t \frac{\eta_i i(\tau)}{C_n}\,\mathrm{d}\tau, \tag{3}$$

where $z(t)$ is the cell SOC, $i(t)$ is instantaneous cell current (assumed positive for discharge, negative for charge), and C_n is the cell nominal capacity. Cell Coulombic efficiency η_i is $\eta_i = 1$ for discharge, and $\eta_i = \eta \leq 1$ for charge.

Using a rectangular approximation for integration and a "suitably small" sampling period Δt, a discrete-time approximate recurrence may then be written as

$$z_{k+1} = z_k - \left(\frac{\eta_i \Delta t}{C_n}\right) i_k. \tag{4}$$

Eq. (4) is the basis for including SOC in the state vector of the cell model as it is in state equation format already, with SOC as the state and i_k as the input.

The cell model may be completed by adding additional states, as necessary, and an output equation. Here, we first revisit an output equation from an earlier paper [5], and show how it may be enhanced. Next, we add a state to the model to account for cell hysteresis. Thirdly, we add dynamics to the state to model cell terminal voltage relaxation. Finally, we discuss adding temperature dependence to the models.

3.3. Models with only SOC as a state

The first three model structures that we investigate have state vector $x_k = z_k$. That is, the only state in the state equation (1) is SOC. These models can estimate cell terminal voltage in a limited way, and are improved upon later using multiple states.

3.3.1. The combined model

With SOC available as part of the model state, terminal voltage may be predicted in a number of different ways. Several different forms are adapted from reference [19].

- *Shepherd model*: $y_k = E_0 - Ri_k - K_i/z_k$.
- *Unnewehr universal model*: $y_k = E_0 - Ri_k - K_i z_k$.
- *Nernst model*: $y_k = E_0 - Ri_k + K_2 \ln(z_k) + K_3 \ln(1 - z_k)$.

In these models, y_k is the cell terminal voltage, R is the cell internal resistance (different values may be used for charge/discharge and at different SOC levels if desired), K_i is the polarization resistance and K_1, K_2 and K_3 are constants chosen to make the model fit the data well. All of the terms of these models may be collected to make a "combined model" that performs better than any of the individual models alone. This model is

$$\begin{aligned} z_{k+1} &= z_k - \left(\frac{\eta_i \Delta t}{C_n}\right) i_k, \\ y_k &= K_0 - Ri_k - \frac{K_1}{z_k} - K_2 z_k + K_3 \ln(z_k) \\ &\quad + K_4 \ln(1 - z_k). \end{aligned}$$

The unknown quantities in the combined model may be estimated using a system identification procedure. This model has the advantage of being "linear in the parameters"; that is, the unknowns occur linearly in the output equation. Given a set of N cell input–output three-tuples $\{y_k, i_k, z_k\}$, the parameters may be solved for in closed form using a result from least-squares estimation. This simple off-line (batch) method is as follows: We first form the vector

$$Y = [y_1, y_2, \ldots, y_N]^T,$$

and the matrix

$$H = [h_1, h_2, \ldots, h_N]^T.$$

The rows of H are

$$h_j^T = \left[1, i_j^+, i_j^-, \frac{1}{z_j}, z_j, \ln(z_j), \ln(1 - z_j)\right],$$

where i_j^+ is equal to i_j if $i_j > 0$, i_j^- is equal to i_j if $i_j < 0$, else i_j^+ and i_j^- are zero. Then, we see that $Y = H\theta$, where $\theta^T = [K_0, R^+, R^-, K_1, K_2, K_3, K_4]$ is the vector of unknown parameters. Using a result from least-squares estimation theory, we solve for the parameters θ using the known matrices Y and H as $\theta = (H^T H)^{-1} H^T Y$.

Results comparing the combined model cell voltage estimation with the cell's true voltage for the pulsed-current test are shown in Fig. 6(a) and (d). Fig. 6(a), shows the comparison over discharge pulses, and Fig. 6(d) shows the comparison over charge pulses. The general shape of the cell response and the model output is the same, although many details of the true cell response are missing. These will be improved with other models. The root-mean-squared model estimation error over the test shown in Fig. 6 is listed in Table 1. Results comparing the combined model cell voltage estimation with the cell's true voltage for one cycle of the UDDS test is shown in Fig. 8(a). Similar comments apply.

3.3.2. The simple model

With parameter values fit to the "combined model", we can evaluate its component terms for further insight. The model output equation may be divided into two additive

Table 1
Performance of the model structures when predicting cell voltage

Model structure	Root-mean-squared (RMS) modeling error			
	Multi-rate pulse test (mV)	Multi-cycle UDDS test (mV)		
		−30 °C	0 °C	25 °C
Combined model	34.7	50.1	24.1	23.3
Simple model	36.2	165.8	26.9	22.4
Zero-state hysteresis model	21.5	62.2	24.6	22.3
One-state hysteresis model	21.5	48.7	14.1	14.0
Enhanced self-correcting, $n_f = 2$	13.8	39.0	14.5	7.2
Enhanced self-correcting, $n_f = 4$	6.7	35.3	4.3	4.2

The root-mean-squared value of modeling error, calculated as true cell voltage minus model voltage, and judged over the SOC range 5–95%, is tabulated.

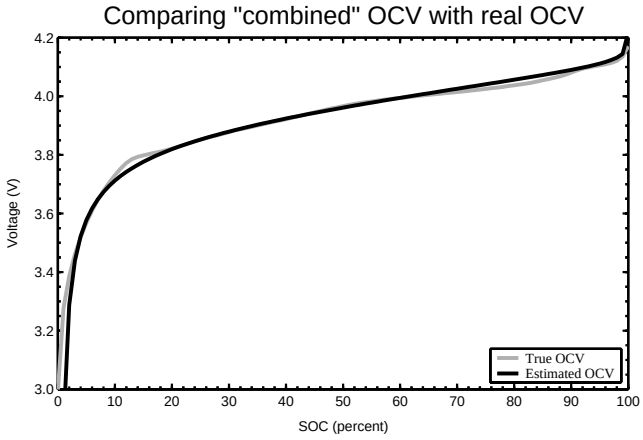

Fig. 3. OCV as a function of SOC, compared with terms from the "combined model."

parts: one part depending only on SOC, and another depending only on i_k:

$$y_k = \underbrace{K_0 - \frac{K_1}{z_k} - K_2 z_k + K_3 \ln(z_k) + K_4 \ln(1 - z_k)}_{\mathrm{fn}(z_k)} - \underbrace{R i_k}_{\mathrm{fn}(i_k)}.$$

The part depending only on SOC bears closer examination. When values are fit to parameters $\{K_0, \ldots, K_4\}$, we plot the part denoted "fn(z_k)" versus z_k (Fig. 3). Overlaid is the open-circuit voltage curve as a function of SOC.[2] We see

[2] The open-circuit voltage as a function of state-of-charge for these cells as plotted in Fig. 3 is an empirical relationship found by cell testing. First, the cell was fully charged (constant current to 4.2 V, constant voltage to 200 mA). Then, the cell was discharged at the $C/25$ rate until fully discharged (3.0 V). The cell was then charged at the $C/25$ rate until the voltage was 4.2 V. The low rates were used to minimize the dynamics excited in the cells. The cell voltage as a function of state of charge under discharge and under charge were averaged to compute the OCV. This has the effect of eliminating to the greatest extent possible the presence of hysteresis and ohmic resistance in the final function. For the purpose of computations involving OCV, the final curve was digitized at 200 points and stored in a table. Linear interpolation is used to look up values in the table.

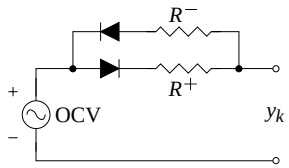

Fig. 4. Equivalent circuit implemented by "simple" model, and approximated by "combined" model. The diodes are ideal. R^+ is the discharge resistance, and R^- is the charge resistance.

that the part of y_k that is a function of SOC is attempting to fit the OCV(z_k) curve. So, an easier and more accurate implementation of the combined model is

$$z_{k+1} = z_k - \left(\frac{\eta_i \Delta t}{C_n}\right) i_k,$$
$$y_k = \mathrm{OCV}(z_k) - R i_k. \quad (5)$$

This output equation is drawn as an equivalent circuit in Fig. 4, where different charge/discharge resistances may be used. We call the model comprised of Eqs. (4) and (5) the "simple model".

This model type is also linear in the parameters. Off-line system identification is done as follows: We first form the vector

$$Y = [y_1 - \mathrm{OCV}(z_1), y_2 - \mathrm{OCV}(z_2), \ldots, y_n - \mathrm{OCV}(z_N)]^T,$$

and the matrix

$$H = [h_1, h_2, \ldots, h_N]^T.$$

The rows of H are

$$h_j^T = [i_j^+, i_j^-].$$

Again, we see that $Y = H\theta$, where $\theta^T = [R^+, R^-]$ is the vector of unknown parameters. We solve for the parameters θ using the known matrices Y and H as $\theta = (H^T H)^{-1} H^T Y$.

Results comparing the simple model cell voltage estimation with the cell's true voltage for the pulsed-current test are shown in Fig. 6(b) and (e). Fig. 6(b), shows the comparison over discharge pulses, and Fig. 6(e) shows the comparison over charge pulses. The RMS cell model estimation

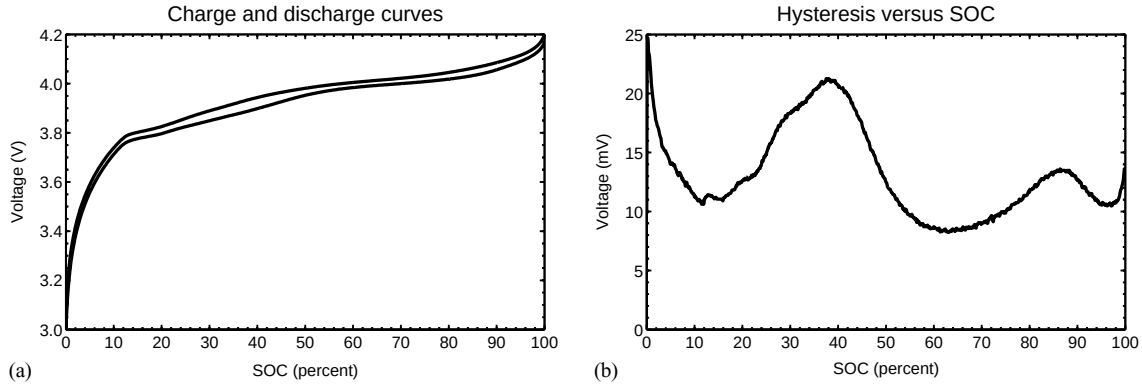

Fig. 5. Hysteresis curves. Plots of: (a) the discharge/charge curves; (b) the hysteresis level.

error over the test shown in Fig. 6 is listed in Table 1. We see that the simple model slightly under-performs the combined model in most cases, most likely because the combined model over-fits the data. We prefer the simple model to the combined model because we feel that it generalizes better, and because it is less complex to implement. Results comparing the simple model cell voltage estimation with the cell's true voltage for one cycle of the UDDS test are shown in Fig. 8(b). Similar comments apply.

3.3.3. The zero-state hysteresis model

Examination of the results in Fig. 6(a) and (b) and (d) and (e) exposes some flaws in the models. One subtle effect, which has serious consequences when predicting SOC, may be seen during rest periods. Following a discharge, the cell voltage always relaxes to a value *less* than the true OCV for that SOC, and following a charge, the cell voltage always relaxes to a value *greater* than the true OCV. This is explained by a hysteresis effect occurring in the cell that is not modeled in the combined or simple models.[3]

The term hysteresis is derived from the Greek *hustereia* "to arrive late". The cell voltage lags the predicted voltage in some sense. It may also be defined as a characteristic of a system in which a change in the direction of the independent variable leads to the dependent variable failing to retrace the path it passed in the forward direction. (For a good paper describing electro-chemical hysteresis, see Ref. [20].)

We illustrate this effect by showing the charge/discharge curves at the $C/25$ rate and room temperature in Fig. 5(a). The terminal voltage for discharge is the lower curve; for charge the upper curve. Two different terminal voltages exist at each SOC. Half the difference between these voltages is the polarization voltage of the cell. Only a small part of the polarization is due to Ri_k drop (about 2.5 mV here) and the remainder is due to hysteresis effects. The hysteresis level, with Ri_k subtracted out, is plotted versus SOC in Fig. 5(b). We have found that cell voltage hysteresis is considerably larger at low temperatures, and that we must include hysteresis in our cell model for good SOC estimation.

These curves comprise the *major hysteresis loop*, corresponding to full cell charge and discharge. Minor hysteresis loops are encountered when a partial charge is followed by a partial discharge, and vice versa. The polarization does not immediately flip sign upon a current reversal, but slowly decays from one leg of the major hysteresis loop to the other.[4] To capture the dynamics of the gradual decay in voltage we need to add one or more states to the model, which is done in Section 3.4.1. Here, we explore a simpler version as a proof-of-concept. This model adds no additional states for hysteresis, so is named the "zero-state hysteresis model".

A basic model of hysteresis simply adds a term to the output equation

$$z_{k+1} = z_k - \left(\frac{\eta_i \Delta t}{C_n}\right) i_k,$$
$$y_k = \mathrm{OCV}(z_k) - s_k M(z_k) - Ri_k,$$

where s_k represents the sign of the current (with memory during a rest period). For some ε sufficiently small and positive,

$$s_k = \begin{cases} 1, & i_k > \varepsilon, \\ -1, & i_k < -\varepsilon, \\ s_{k-1}, & |i_k| \le \varepsilon. \end{cases}$$

$M(z_k)$ is half the difference between the two legs of the charge/discharge curve, minus the Ri_k loss, and is plotted in Fig. 5(b). Here, we use a constant value for M.

[3] We note in passing that hysteresis is not a phenomenon generally associated with lithium-ion systems, since most applications have been in the light portable electronics area where SOC accuracy is not as critical as in the HEV application and where temperatures are not as extreme. It is, however, very pronounced at low temperatures and can lead to SOC errors as large as ±40% if the estimate is based simply on OCV (even with full cell relaxation). The reason is the spread between the charge and discharge characteristics coupled with the flat nature of the curves between 10 and 90% SOC.

[4] Successively smaller concentric minor loops may be obtained by alternating shorter and shorter charge and discharge pulses, eventually converging on the mean of the two values of Fig. 5(a) at each SOC. Therefore, we compute OCV as a function of SOC as the mean of the two legs of the major hysteresis loop.

This model type is also linear in the parameters. Off-line system identification is done as follows: We first form the vector

$$Y = [y_1 - \mathrm{OCV}(z_1), y_2 - \mathrm{OCV}(z_2), \ldots, y_n - \mathrm{OCV}(z_N)]^T,$$

and the matrix

$$H = [h_1, h_2, \ldots, h_N]^T.$$

The rows of H are

$$h_j^T = [i_j^+, i_j^-, s_j].$$

Again, we see that $Y = H\theta$, where $\theta^T = [R^+, R^-, M]$ is the vector of unknown parameters. We solve for the parameters θ using the known matrices Y and H as $\theta = (H^T H)^{-1} H^T Y$.

Results comparing the zero-state hysteresis model cell voltage estimation with the cell's true voltage for the pulsed-current test are shown in Figs. 6(c) and (f). Fig. 6(c), shows the comparison over discharge pulses, and Fig. 6(f) shows the comparison over charge pulses. The RMS cell model estimation error over the test shown in Fig. 6 is listed in Table 1. Performance of the zero-state hysteresis model is consistently better than that of the simple model. Results comparing the zero-state hysteresis model cell voltage estimation with the cell's true voltage for one cycle of

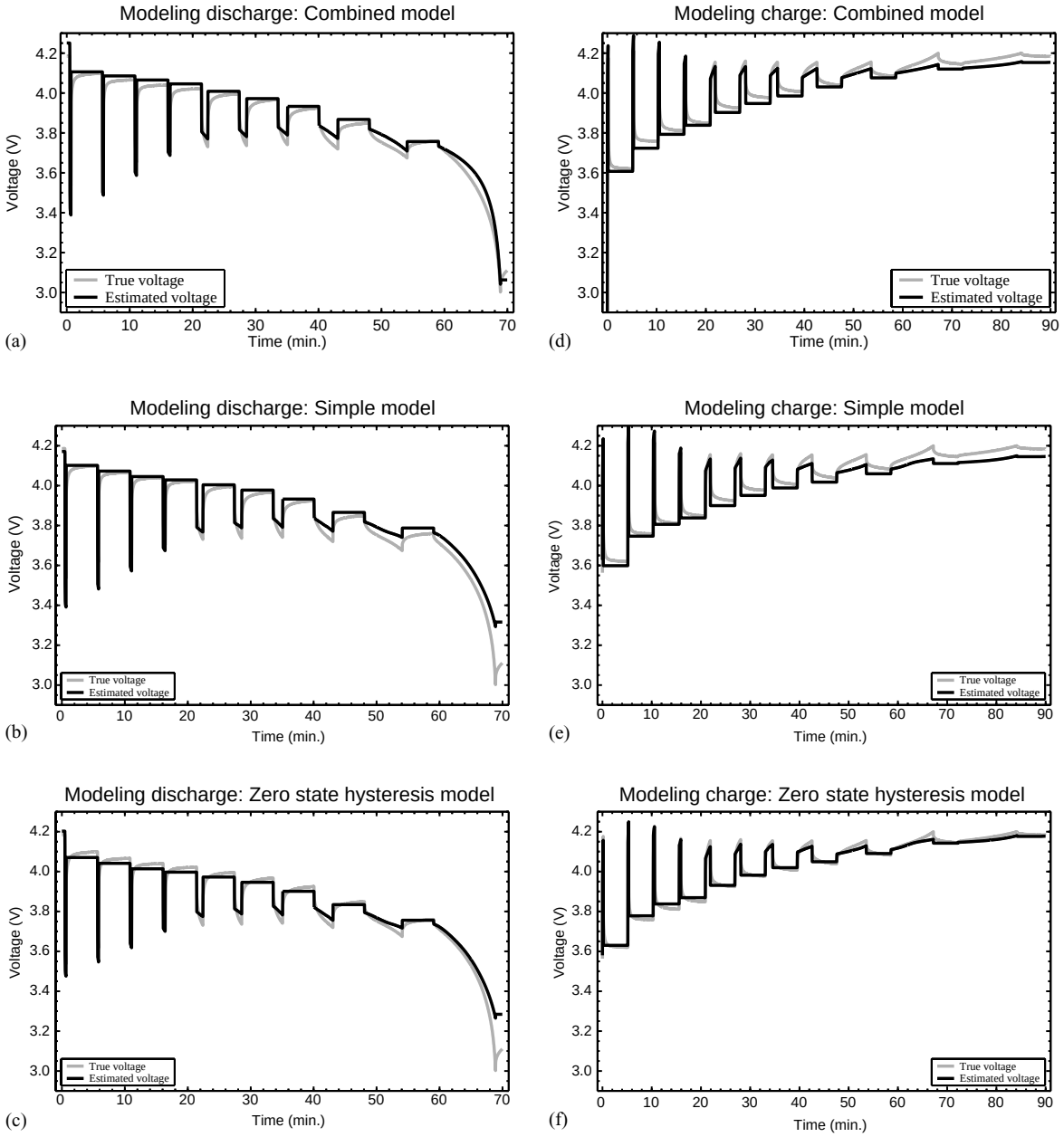

Fig. 6. Results of cell modeling using models with only SOC as a state for the pulsed-current cell tests. Discharge portion of test is shown in (a)–(c); charge portion of test is shown in (d)–(f). The gray line is the measured cell voltage, and the black line is the model prediction.

the UDDS test are shown in Fig. 8(c). Similar comments apply.

3.4. Models with SOC and additional states

In order to better estimate cell voltage effects that are coupled to the history of the cell's input current, we must make modifications to the model state equation (1). We examine two additions in the following sections.

3.4.1. The one-state hysteresis model

The zero-state hysteresis model is an improvement over the simple model, but only crudely approximates the underlying phenomenon. Whereas the level of hysteresis slowly changes as the cell is charged or discharged, the model estimates hysteresis as immediately flipping between its maximum positive and negative values when the sign of current changes.

The slow transition may be modeled by adding a "hysteresis state" to the model state equation (1). The hysteresis state is not a differential equation in time, but in SOC (or, ampere-hours). Let $h(z,t)$ be the hysteresis voltage as a function of SOC and time, and let $\dot{z} = \mathrm{d}z/\mathrm{d}t$. Then,

$$\frac{\mathrm{d}h(z,t)}{\mathrm{d}z} = \gamma \operatorname{sgn}(\dot{z})(M(z,\dot{z}) - h(z,t)),$$

where $M(z,\dot{z})$ is a function that gives the maximum polarization due to hysteresis as a function of SOC and the rate-of-change of SOC. Specifically, $M(z,\dot{z})$ is positive for charge ($\dot{z} > 0$) and is negative for discharge ($\dot{z} < 0$). The $M(z,\dot{z}) - h(z,t)$ term in the differential equation states that the rate-of-change of hysteresis voltage is proportional to the distance away from the major hysteresis loop, leading to a kind of exponential decay of voltage to the major loop. The term in front of this has a positive constant γ, which tunes the rate of decay, and $\operatorname{sgn}(\dot{z})$, which forces the equation to be stable for both charge and discharge.

In order to fit the differential equation for $h(z,t)$ into our model, we must manipulate it to be a differential equation in time, not in SOC. We accomplish this by multiplying both sides of the equation by $\mathrm{d}z/\mathrm{d}t$

$$\frac{\mathrm{d}h(z,t)}{\mathrm{d}z}\frac{\mathrm{d}z}{\mathrm{d}t} = \gamma \operatorname{sgn}(\dot{z})(M(z,\dot{z}) - h(z,t))\frac{\mathrm{d}z}{\mathrm{d}t}.$$

Note that $\mathrm{d}z/\mathrm{d}t = -\eta_i i(t)/C_\mathrm{n}$, and that $\dot{z}\operatorname{sgn}(\dot{z}) = |\dot{z}|$. Thus,

$$\dot{h}(t) = -\left|\frac{\eta_i i(t)\gamma}{C_\mathrm{n}}\right| h(t) + \left|\frac{\eta_i i(t)\gamma}{C_\mathrm{n}}\right| M(z,\dot{z}).$$

This may be converted into a difference equation for our discrete-time application using standard techniques (assuming that $i(t)$ and $M(z,\dot{z})$ are constant over the sample period):

$$h_{k+1} = \exp\left(-\left|\frac{\eta_i i_k \gamma \Delta t}{C_\mathrm{n}}\right|\right) h_k + \left(1 - \exp\left(-\left|\frac{\eta_i i_k \gamma \Delta t}{C_\mathrm{n}}\right|\right)\right) M(z,\dot{z}).$$

Note that this is a linear-time-varying system as the factors multiplying the state and input change with i_k and hence with time. If we define $F(i_k) = \exp(-|\eta_i i_k \gamma \Delta t/C_\mathrm{n}|)$, then the overall state-space equations for the one-state hysteresis model are

$$\begin{bmatrix} h_{k+1} \\ z_{k+1} \end{bmatrix} = \begin{bmatrix} F(i_k) & 0 \\ 0 & 1 \end{bmatrix} \begin{bmatrix} h_k \\ z_k \end{bmatrix} + \begin{bmatrix} 0 & (1 - F(i_k)) \\ -\dfrac{\eta_i \Delta t}{C_\mathrm{n}} & 0 \end{bmatrix} \begin{bmatrix} i_k \\ M(z,\dot{z}) \end{bmatrix},$$

$$y_k = \mathrm{OCV}(z_k) - Ri_k + h_k.$$

Results comparing the one-state hysteresis model cell voltage estimation with the cell's true voltage for the pulsed-current test are shown in Fig. 7(a) and (d). Fig. 7(a), shows the comparison over discharge pulses, and Fig. 7(d) shows the comparison over charge pulses. The RMS cell model estimation error over the test shown in Fig. 7 is listed in Table 1. Performance of the one-state hysteresis model is consistently better than the simpler models. Results comparing the one-state hysteresis model cell voltage estimation with the cell's true voltage for one cycle of the UDDS test are shown in Fig. 8(d). Similar comments apply.

3.4.2. The enhanced self-correcting (ESC) model

A significant element missing from these models is a description of time constants during pulsed current events. If a cell is allowed to rest, it takes some time for the voltage to completely relax to its rest voltage. If a cell is pulsed with current, it takes time for the voltage to converge to its steady-state level. These time constants, which describe the phenomenon we henceforth refer to as the relaxation effect, may be implemented as a low-pass filter on i_k. Since the cell model must accurately predict its behavior in a dynamic HEV environment, we find it is essential to include relaxation effects.

Early attempts to model the relaxation effect included filtering the state-of-charge as well as the input current (cf. the "filter state" cell model [5]). While this model could fit voltage data reasonably well, it had the unfortunate side effect that SOC estimation using an EKF was not reliable. The output equation had the form

$$y_k = \mathrm{OCV}(z_k) + \mathrm{filt}(z_k) + \mathrm{filt}(i_k) - Ri_k,$$

where $\mathrm{filt}(\cdot)$ is some dynamic operation filtering its operand. The EKF had problems with this model because the credit/blame portion of the algorithm could not reliably determine whether model error was due to bad SOC through the $\mathrm{OCV}(\cdot)$ function or through the $\mathrm{filt}(z_k)$ function, or due to bad filter states in the $\mathrm{filt}(i_k)$ function. In particular, some simple cell tests running the EKF showed a lack of robustness:

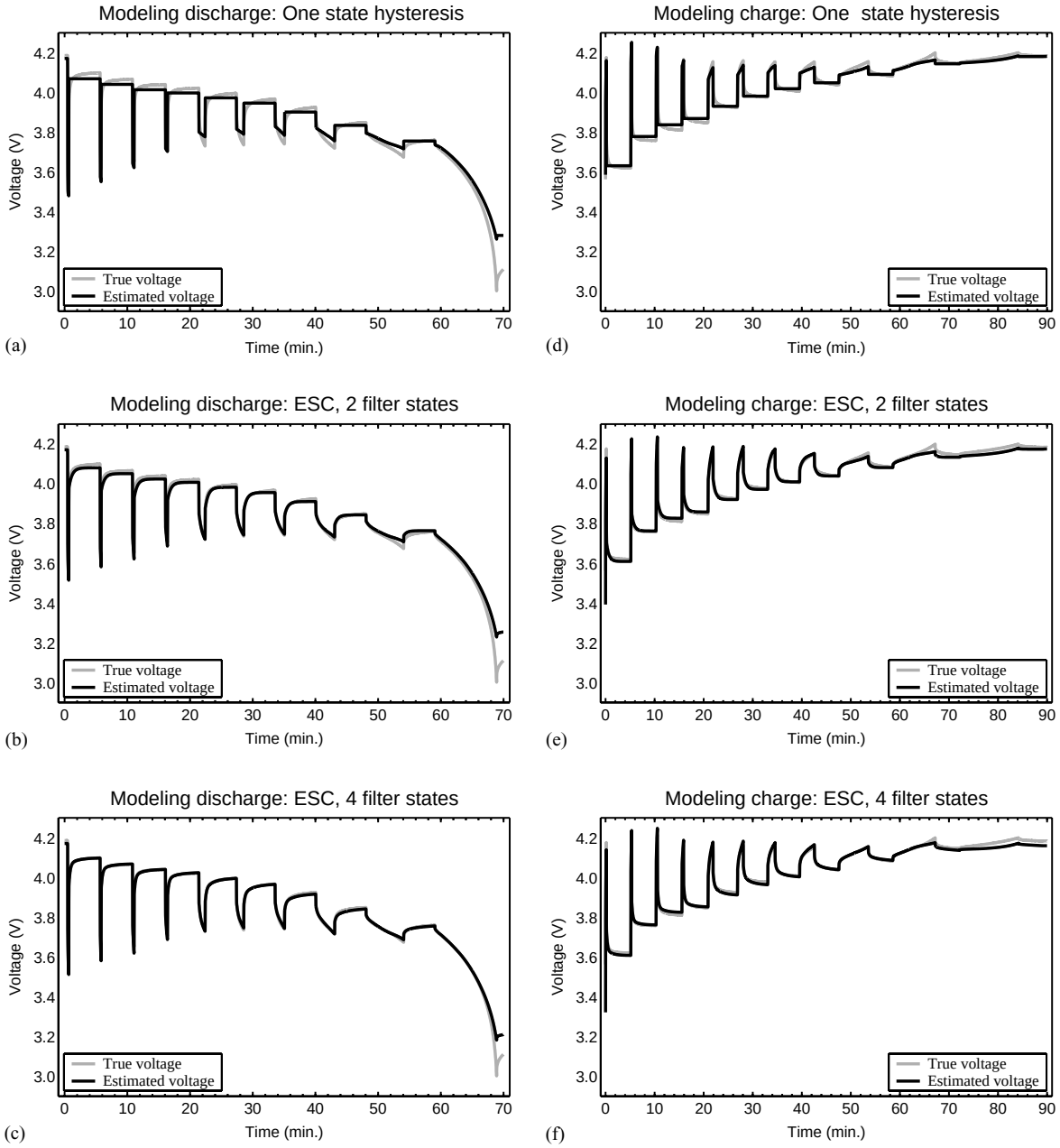

Fig. 7. Results of cell modeling using models with multiple states for the pulsed-current cell tests. Discharge portion of test is shown in (a)–(c); charge portion of test is shown in (d)–(f). The gray line is the measured cell voltage, and the black line is the model prediction.

1. A constant-current discharge/charge should make the SOC ramp down/up at the slope i/C_n (A/Ah). In practice, the slope using the filter state model was often wrong.
2. During a rest period, cell terminal voltage converges to OCV (neglecting hysteresis effects) and estimated SOC should converge to the SOC predicted by OCV. In the implementation, we observed SOC to drift considerably, not converging to the correct value.

The model that we will develop in this section, called the "enhanced self-correcting model", forces y_k to converge to OCV after a rest period and it forces y_k to converge to $\mathrm{OCV} - Ri_k$ for a constant-current discharge/charge. To meet these requirements, with hysteresis added, the output equation needs to have the form

$$y_k = \underbrace{\mathrm{OCV}(z_k)}_{\mathrm{fn}(z_k)} + \underbrace{h_k}_{\mathrm{fn}(z_k, i_k)} + \underbrace{\mathrm{filt}(i_k) - Ri_k}_{\mathrm{fn}(i_k)}.$$

In this equation, SOC and hysteresis contribute the long-term dc level (bias) to the output and i_k and its history contribute the short-term variation around this level. SOC itself is no longer filtered as in the "filter state model"—it makes no sense to have a moving bias point.

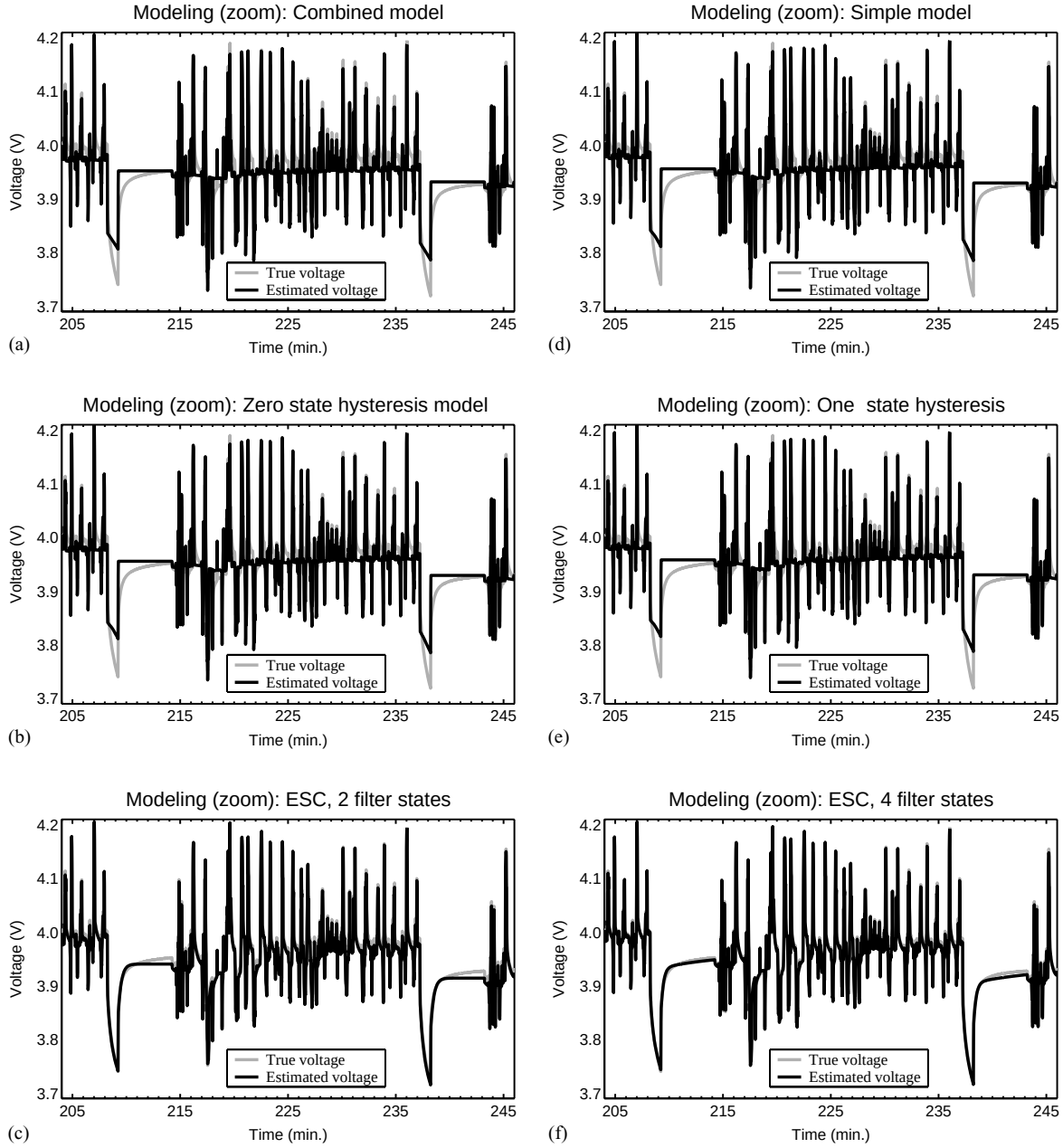

Fig. 8. Results of cell modeling for the UDDS cell tests. The gray line is the measured cell voltage, and the black line is the model prediction.

The filter "filt(·)" must satisfy two criteria: (1) after a long rest period its output must be zero so that $y_k \rightarrow \text{OCV} + h_k$; (2) during a constant-current discharge/charge, its output must converge to zero so that $y_k \rightarrow \text{OCV} + h_k - Ri_k$. The first criterion is satisfied by a stable linear filter, and the second is satisfied by a linear filter with zero dc gain. Both of these may be enforced in the filter design.

A linear filter may be implemented in a state-space form as

$$f_{k+1} = A_\text{f} f_k + B_\text{f} i_k,$$
$$y_k^\text{f} = G f_k,$$

where A_f is the state-transition matrix of the filter, B_f is the input matrix of the filter, G is the output matrix of the filter, and f_k is the filter state. The eigenvalues of the A_f matrix are the "poles" of the filter and determine its stability. The filter is stable if $\max|\text{eig}(A_\text{f})| < 1$. The location of poles determine the system's dynamic behavior: poles near $+1$ have slowly decaying dynamics, poles near zero decay quickly, negative poles oscillate. Complex-conjugate poles also oscillate, and do not appear to improve performance by their inclusion. Therefore, it is sufficient to have an A_f matrix of the form $A_\text{f} = \text{diag}(\alpha)$, where α is a vector comprising the pole locations. Stability is ensured if all $-1 < \alpha_j < 1$. The B_f matrix may be chosen arbitrarily so long as no entry is zero.

Now that we have guaranteed stability, $y_k \rightarrow \mathrm{OCV} + h_k$ during rest. By carefully selecting the G matrix, we can ensure a zero dc-gain of the filter so that $y_k \rightarrow \mathrm{OCV} + h_k - Ri_k$ during constant-current profiles. The gain of the filter is (where n_f is the number of filter states, determined during system identification to fit cell data):

$$G(I - A)^{-1}B = 0,$$
$$G\left[\mathrm{diag}\left(\frac{1}{1-\alpha_k}\right)\right]B = 0,$$
$$\sum_{k=1}^{n_\mathrm{f}} \frac{g_k}{1-\alpha_k} = 0.$$

If we let g_1 through $g_{n_\mathrm{f}-1}$ be found by a system-identification procedure and assuming that $B_\mathrm{f} = [\,1 \quad \cdots \quad 1\,]^\mathrm{T}$, then the zero dc-gain constraint fixes g_{n_f} as

$$g_{n_\mathrm{f}} = -\sum_{k=1}^{n_\mathrm{f}} g_k \frac{(1-\alpha_{n_\mathrm{f}})}{(1-\alpha_k)}.$$

So, the full self-correcting model is

$$\begin{bmatrix} f_{k+1} \\ h_{k+1} \\ z_{k+1} \end{bmatrix} = \begin{bmatrix} \mathrm{diag}(\alpha) & 0 & 0 \\ 0 & F(i_k) & 0 \\ 0 & 0 & 1 \end{bmatrix} \begin{bmatrix} f_k \\ h_k \\ z_k \end{bmatrix} + \begin{bmatrix} 1 & 0 \\ 0 & (1-F(i_k)) \\ -\dfrac{\eta_i \Delta t}{C_\mathrm{n}} & 0 \end{bmatrix} \begin{bmatrix} i_k \\ M(z,\dot{z}) \end{bmatrix},$$
$$y_k = \mathrm{OCV}(z_k) - Ri_k + h_k + Gf_k.$$

Results comparing the ESC model cell voltage estimation with the cell's true voltage for the pulsed-current test are shown in Figs. 7(b) and (e) for $n_\mathrm{f} = 2$ and in Figs. 7(c) and (f) for $n_\mathrm{f} = 4$. Figs. 7(b) and (c), show the comparison over discharge pulses, and Figs. 7(e) and (f) show the comparison over charge pulses. The RMS cell model estimation error over the tests shown in Fig. 7 are listed in Table 1. Performance is significantly improved by the addition of filter states. We do not see much improvement by increasing n_f beyond 4. Results comparing the ESC model cell voltage estimation with the cell's true voltage for one cycle of the UDDS test are shown in Figs. 8(e) for $n_\mathrm{f} = 2$ and (f) for $n_\mathrm{f} = 4$.

3.5. Adding temperature dependence to the models

Thus far, we have discussed only how to model cell dynamics at one specific temperature. We now embark on a brief discussion on how to incorporate temperature dependence into the models.

A very simple method, and the one we tried first, was to use a table of different models, where each model had parameters optimized for a specific temperature. For example, we used sixteen models over the temperature range −30 to 45 °C in increments of 5 °C. This worked well so long as the cell under test had temperature equivalent to one of the sixteen stored models. If the temperature was between two stored model values, we linearly interpolated model parameters between the parameters of the models in the table. This did not work well.

We found that two adjacent models in the table did not necessarily have similar parameters. Individually optimizing model parameters at specific temperatures resulted in values that were over-fit to the data and did not generalize well to cases not previously seen. We remedied the problem by performing joint optimization over the entire temperature range, where every parameter was represented by a continuous polynomial of temperature (fourth order). This forced nearby models to have similar parameter values. Although joint optimization did not result in modeling errors as low as when individually optimized, the generalization performance was much better.

Fig. 9 shows the results for joint optimization over the entire temperature range, and Table 1 lists some numeric values corresponding to the plots. The cell data was collected from UDDS tests similar to those described in Section 3.1, but performed at 16 controlled temperatures from −30 to 45 °C, in increments of 5°C. At lower temperatures, the magnitude of the current had to be scaled down so as not to exceed voltage limits (due to increased cell

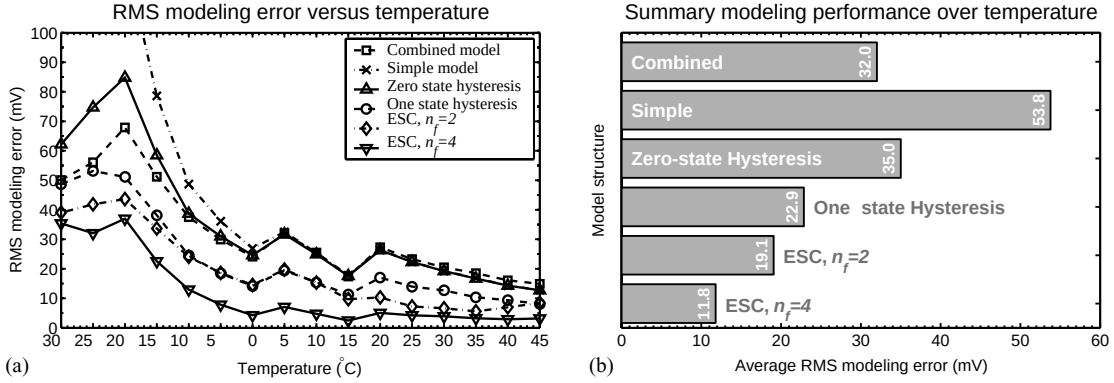

Fig. 9. Results when modeling over a temperature range. Frame (a) shows the individual modeling results, and frame (b) compares the average modeling results.

resistance at lower temperatures), and hence more UDDS cycles had to be completed to cover the desired SOC range, but the tests were otherwise the same. In frame (a), the RMS modeling errors for the jointly optimized models are plotted versus temperature for the different cell models. In frame (b), the average RMS modeling errors over all temperatures are presented as a bar graph.

We see that the combined model appears to perform well. However, this is an artifact. The $\{K_0, \ldots, K_4\}$ points were found to over-fit the measured data, so that the resulting curve plotted with their values did not resemble OCV to any degree of fidelity. While the simple model has worse numeric indicators of performance, it generalized better than the combined model. By adding the crude model of hysteresis, we see a significant performance jump, especially at cold temperatures where hysteresis is most evident in our cells' dynamics. Adding the dynamics of a state to the hysteresis model also improves performance, again with the greatest gains at low temperatures. Filter states also contribute to performance gains. The final model, enhanced-self-correcting with $n_f = 4$ gave the best performance in all cases. By increasing the number of filter states we would expect continued performance gains, at the cost of greater complexity. Note that the cold-temperature performance is not improved as much, in relative terms, by adding filter states, so it is likely that some cold-temperature phenomena is not yet being modeled well. Conceivably, a second hysteresis state could be added to the model to improve performance here. We have not investigated this possibility as yet.

4. System identification

The first three system models introduced in this paper are "linear in the parameters". This makes identifying the values of the model parameters straightforward using least-squares estimation, and has been discussed earlier. When the model is not linear in the parameters, as in the remaining system models, this method may not be used. We must turn to more advanced methods.

Here we look at one method in particular. We know that a Kalman filter or extended Kalman filter may be used to estimate the state of a dynamic system given noisy measurements; e.g., to estimate the cell SOC. We may also use an extended Kalman filter to perform system identification given clean measurements. To do so, we require a state-space model describing the dynamics of the parameters θ of the system model. We will use the Kalman filter as an optimum observer of these parameter values, creating an estimate $\hat{\theta}$. In electro-chemical cells, the true parameters will change only very slowly, so we model them as constant with some small perturbation:

$$\theta_{k+1} = \theta_k + r_k.$$

The small white noise input r_k is fictitious, but models the slow change in the parameters of the system plus the infidelity of the model structure to capture all of the cell dynamics.

Table 2
Summary of the nonlinear extended Kalman filter for system identification [21]

Nonlinear state-space model[a]

$$\theta_{k+1} = \theta_k + r_k$$
$$d_k = g(x_k, u_k, \theta_k) + e_k$$

Definition

$$C_k^\theta = \left.\frac{\mathrm{d}g(x_k, u_k, \theta)}{\mathrm{d}\theta}\right|_{\theta=\hat{\theta}_k^-}$$

Initialization

For $k = 0$, set

$$\hat{\theta}_0^+ = \mathbb{E}[\theta_0]$$
$$\Sigma_{\tilde{\theta},0}^+ = \mathbb{E}[(\theta_0 - \hat{\theta}_0^+)(\theta_0 - \hat{\theta}_0^+)^{\mathrm{T}}]$$

Computation

For $k = 1, 2, \ldots$ compute

State estimate time update: $\hat{\theta}_k^- = \hat{\theta}_{k-1}^+$

Error covariance time update: $\Sigma_{\tilde{\theta},k}^- = \Sigma_{\tilde{\theta},k-1}^+ + \Sigma_r$

Kalman gain matrix: $L_k^\theta = \Sigma_{\tilde{\theta},k}^-(C_k^\theta)^{\mathrm{T}}[C_k^\theta \Sigma_{\tilde{\theta},k}^-(C_k^\theta)^{\mathrm{T}} + \Sigma_e]^{-1}$

State estimate measurement update: $\hat{\theta}_k^+ = \hat{\theta}_k^- + L_k[y_k - g(x_k, u_k, \hat{\theta}_k^-)]$

Error covariance measurement update: $\Sigma_{\tilde{\theta},k}^+ = (I - L_k^\theta C_k^\theta)\Sigma_{\tilde{\theta},k}^-$

[a] r_k and e_k are independent, zero-mean, Gaussian noise processes of covariance matrices Σ_r and Σ_e, respectively.

The output equation required for Kalman-filter system identification must be a measurable function of the system parameters. We use

$$d_k = g(x_k, u_k, \theta_k) + e_k,$$

where $g(\cdot, \cdot, \cdot)$ is the output equation of the system model being identified, and e_k models the sensor noise and modeling error. We compare d_k computed using $\hat{\theta}_k$ to the measured cell output, and adapt $\hat{\theta}_k$ to minimize the difference.

We can create an extended Kalman filter using this state-space model and cell data to estimate the system parameters as summarized in Table 2. We initialize the state estimate with our best information re. the state value: $\hat{\theta}_0^+ = \mathbb{E}[\theta_0]$, and the state estimation error covariance matrix: $\Sigma_{\tilde{\theta},0}^+ = \mathbb{E}[(\theta - \hat{\theta}_0^+)(\theta - \hat{\theta}_0^+)^{\mathrm{T}}]$.

The time update propagates the state estimate as $\hat{\theta}_k^- = \hat{\theta}_{k-1}^+$ since the parameters are assumed constant, and the error covariance as $\Sigma_{\tilde{\theta},k}^- = \Sigma_{\tilde{\theta},k-1}^+ + \Sigma_r$ to account for the added uncertainty due to the fictitious noise input r_k. The effect of adding Σ_r is to increase the estimate's uncertainty, and to allow adaptation to $\hat{\theta}$.

The extended Kalman filter gain matrix is computed by linearizing the state-space model's output equation. We compute

$$C_k^\theta = \left.\frac{\mathrm{d}g(x_k, u_k, \theta)}{\mathrm{d}\theta}\right|_{\theta=\hat{\theta}_k^-},$$
$$L_k^\theta = \Sigma_{\tilde{\theta},k}^-(C_k^\theta)^{\mathrm{T}}[C_k^\theta \Sigma_{\tilde{\theta},k}^-(C_k^\theta)^{\mathrm{T}} + \Sigma_e]^{-1}.$$

Next, we measure the true cell output y_k and compare it to the model output $g(x_k, u_k, \hat{\theta}_k^-)$. To do so, we need to simulate the model in parallel with the real cell to have an appropriate value of x_k available. The difference between cell output and model output can be attributed to noises and modeling error. The extended Kalman filter adapts $\hat{\theta}$ to minimize this difference

$$\hat{\theta}_k^+ = \hat{\theta}_k^- + L_k[y_k - g(x_k, u_k, \hat{\theta}_k^-)].$$

Finally, the measurement update is applied to the state error covariance matrix

$$\Sigma_{\tilde{\theta},k}^+ = (I - L_k^\theta C_k^\theta)\Sigma_{\tilde{\theta},k}^-.$$

This has the effect of decreasing the modeling uncertainty due to the measurement update. All terms are accounted for, and the algorithm is complete.

4.1. Extended Kalman-filter system identification for the one-state hysteresis model

The details for applying this method to any particular cell model are differentiated by the calculation of C_k^θ. For the one-state hysteresis model, let the vector of parameters be

$$\theta = [\, R^+ \quad R^- \quad M \quad \gamma \,]^{\mathrm{T}}.$$

R^+ is the cell resistance when current is positive, and R^- is the cell resistance when current is negative. M is the maximum hysteresis voltage, and γ is the hysteresis rate constant, which is part of $F(i_k)$. To calculate C_k^θ we require

$$\frac{\mathrm{d}g(x_k, u_k, \theta)}{\mathrm{d}\theta} = \frac{\partial g(x_k, u_k, \theta)}{\partial \theta} + \frac{\partial g(x_k, u_k, \theta)}{\partial x_k}\frac{\mathrm{d}x_k}{\mathrm{d}\theta}, \tag{6}$$

$$\frac{\mathrm{d}x_k}{\mathrm{d}\theta} = \frac{\partial f(x_{k-1}, u_{k-1}, \theta)}{\partial \theta} + \frac{\partial f(x_{k-1}, u_{k-1}, \theta)}{\partial x_{k-1}}\frac{\mathrm{d}x_{k-1}}{\mathrm{d}\theta}. \tag{7}$$

The derivative calculations are recursive in nature, and evolve over time as the state evolves. The term $\mathrm{d}x_0/\mathrm{d}\theta$ is initialized to zero unless side information gives a better estimate of its value. We see that in order to calculate C_k^θ for any specific model structure, we require methods to calculate the partial derivatives in (6) and (7). For the one-state hysteresis model we have

$$\frac{\partial g(x_k, u_k, \theta)}{\partial \theta} = [\, -i^+ \quad -i^- \quad 0 \quad 0 \,], \qquad \frac{\partial g(x_k, u_k, \theta)}{\partial x_k} = \begin{bmatrix} 1 & \dfrac{\partial \mathrm{OCV}(z_k)}{\partial z_k} \end{bmatrix},$$

$$\frac{\partial f(x_{k-1}, u_{k-1}, \theta)}{\partial \theta} = \begin{bmatrix} 0 & 0 & (1 - F_{k-1})\,\mathrm{sgn}(i_{k-1}) & (M - h_{k-1})\left|\dfrac{\eta_i i_{k-1}\Delta t}{C}\right| F_{k-1} \\ 0 & 0 & 0 & 0 \end{bmatrix}, \qquad \frac{\partial f(x_{k-1}, u_{k-1}, \theta)}{\partial x_{k-1}} = \begin{bmatrix} F_{k-1} & 0 \\ 0 & 1 \end{bmatrix}.$$

Note that the $\partial \mathrm{OCV}(z_k)/\partial z_k$ term is never needed, as it always multiplies zero. For this particular model, we can simplify the calculations by removing the multiplies by zero:

$$\frac{\mathrm{d}g(x_k, u_k, \theta)}{\mathrm{d}\theta} = [\, -i^+ \quad -i^- \quad 0 \quad 0 \,] + \frac{\mathrm{d}h_k}{\mathrm{d}\theta}, \qquad \frac{\mathrm{d}h_k}{\mathrm{d}\theta} = \begin{bmatrix} 0 & 0 & (1 - F_{k-1})\,\mathrm{sgn}(i_{k-1})(M - h_{k-1})\left|\dfrac{\eta_i i_{k-1}\Delta t}{C}\right| F_{k-1} \end{bmatrix} + F_{k-1}\frac{\mathrm{d}h_{k-1}}{\mathrm{d}\theta}.$$

4.2. Extended Kalman-filter system identification for the enhanced self-correcting model

For the enhanced self-correcting model, let the vector of parameters be

$$\theta = [\, R^+ \quad R^- \quad g_1 \quad \cdots \quad g_{n_\mathrm{f}-1} \quad \beta_1 \quad \cdots \quad \beta_{n_\mathrm{f}} \quad M \quad \gamma \,]^{\mathrm{T}},$$

where $\beta = \tanh(\alpha)$ and α is the vector of filter pole locations. We use the $\tanh(\cdot)$ function during system identification because it forces filter poles to remain within ± 1 (i.e., stable) regardless of the value of β. When calculating the partial derivatives we must remember that since $g_{n_\mathrm{f}} = -\sum_{i=1}^{n_\mathrm{f}-1} g_i(1 - \alpha_{n_\mathrm{f}})/(1 - \alpha_i)$, it is not independently identified but is computed from the $g_1, \ldots, g_{n_\mathrm{f}-1}$ terms. This also forces the derivatives to be more complicated than a quick glance would indicate. That is,

$$\frac{\partial g(x_k, u_k, \theta)}{\partial g_1} = f_{k,1} - \frac{1 - \alpha_{n_\mathrm{f}}}{1 - \alpha_1} f_{k,n_\mathrm{f}},$$

and so forth. Also, since $\alpha_i = \tanh(\beta_i)$, it can never be unity, so division by zero is impossible in the derivative computation. With this in mind, the partial derivatives in (6) and (7) may be computed in a straightforward way.

5. Conclusions

This paper has proposed five mathematical state-space structures for the purpose of modeling LiPB HEV cell dynamics for their eventual role in HEV BMS algorithms. Models with a single-state are very simple, but perform the poorest. Adding hysteresis and filter states to the model aids performance, at some cost in complexity.

We have also seen how to identify the parameters of the cell models given cell-test data. Models that are "linear in the parameters" may have their parameters fit in a very straightforward way using methods from least-squares-estimation theory. Models with more dynamics than simply SOC require more sophisticated techniques. One possibility is to use an extended Kalman filter to identify the cell parameters in an on-line or off-line manner.

In the third paper [4], we will employ extended Kalman filtering from [3], using the cell models developed here, to implement HEV BMS algorithms. We will see how to use EKF to estimate SOC and all other model states as the system operates. This model state will then allow us to accurately compute a dynamic estimate of available power. We can additionally employ a technique called *dual extended Kalman filtering* to simultaneously estimate cell state and parameters, allowing tracking of cell power fade and capacity fade, for example. Finally, the parameter data and SOC estimate may be combined to determine which cells in the pack must have their charge levels modified in order to bring the pack into equalization.

Acknowledgements

This work was supported in part by Compact Power Inc. (CPI). The use of company facilities, and many enlightening discussions with Drs. Mohamed Alamgir and Dan Rivers and others are gratefully acknowledged.

References

[1] C. Barbier, H. Meyer, B. Nogarede, S. Bensaoud, A battery state of charge indicator for electric vehicle, in: Proceedings of the International Conference of the Institution of Mechanical Engineers, Automotive Electronics, London, UK, 17–19 May 1994, pp. 29–34.
[2] P. Lürkens, W. Steffens, Ladezustandsschätzung von bleibatterien mit hilfe des Kalman-filters (State of charge estimation of lead-acid batteries using a Kalman filtering technique), etzArchiv, vol. 8, No. 7, July 1986, pp. 231–236 (in German).
[3] G. Plett, Extended Kalman filtering for battery management systems of LiPB-based HEV battery packs. Part 1. Background, J. Power Sour. 134 (2) (2004) 252–261.
[4] G. Plett, Extended Kalman filtering for battery management systems of LiPB-based HEV battery packs. Part 3. State and parameter estimation, J. Power Sour. 134 (2) (2004) 277–292.
[5] G. Plett, LiPB dynamic cell models for Kalman-filter SOC estimation, in: Proceedings of the EVS-19, Busan, Korea, October 2002 (CD-ROM).
[6] G. Plett, Advances in EKF SOC estimation for LiPB HEV battery packs, in: Proceedings of the EVS-20, Long Beach, CA, November 2003.
[7] S. Piller, M. Perrin, A. Jossen, Methods for state-of-charge determination and their applications, J. Power Sour. 96 (2001) 113–120.
[8] W.B. Gu, C.Y. Wang, Thermal–electrochemical modeling of battery systems, J. Electrochem. Soc. 147 (8) (2000) 2910–2922.
[9] K. Takano, K. Nozaki, Y. Saito, A. Negishi, K. Kato, Y. Yamaguchi, Simulation study of electrical dynamic characteristics of lithium-ion battery, J. Power Sour. 90 (2) (2000) 214–223.
[10] E. Barsoukov, J. Kim, C. Yoon, H. Lee, Universal battery parameterization to yield a non-linear equivalent circuit valid for battery simulation at arbitrary load, J. Power Sour. 83 (1/2) (1999) 61–70.
[11] S. Rodrigues, N. Munichandraiah, A. Shukla, A review of state-of-charge indication of batteries by means of ac impedance measurements, J. Power Sour. 87 (1/2) (2000) 12–20.
[12] A. Salkind, C. Fennie, P. Singh, T. Atwater, D. Reisner, Determination of state-of-charge and state-of-health of batteries by fuzzy logic methodology, J. Power Sour. 80 (1/2) (1999) 293–300.
[13] P. Singh, C. Fennie, D. Reisner, A. Salkind, Fuzzy logic-enhanced electrochemical impedance spectroscopy (fleeis) to determine battery state of charge, in: Proceedings of the 15th Annual Battery Conference on Applications and Advances, Long Beach, CA, USA, 11–14 January 2000, pp. 199–204.
[14] A. Kawamura, T. Yanagihara, State of charge estimation of sealed lead-acid batteries used for electric vehicles, in: Proceedings of the 29th Annual IEEE Power Electronics Specialists Conference, Fukuoka, Japan, 17–22 May 1998, pp. 583–587.
[15] S. Bhatikar, R. Mahajan, K. Kipke, V. Johnson, Neural network based battery modeling for hybrid electric vehicles, in: Proceedings of the 2000 Future Car Congress, Paper No. 2000-01-1564, Arlington, VA, 2–6 April 2000.
[16] H. Chan, D. Sutanto, A new battery model for use with battery energy storage systems and electric vehicle power systems, in: Proceedings of the 2000 IEEE Power Engineering Society Winter Meeting, Singapore, 23–27 January 2000, pp. 470–475.
[17] V. Johnson, A. Pesaran, T. Sack, Temperature-dependent battery models for high-power lithium-ion batteries, in: Proceedings of the 17th Electric Vehicle Symposium, Montreal, Canada, 15–18 October 2000.
[18] R. Giglioli, P. Pelacchi, M. Raugi, G. Zini, A state of charge observer for lead-acid batteries, Energia Elettrica 65 (1) (1988) 27–33.
[19] ThermoAnalytics Inc., Battery modeling for HEV simulation by ThermoAnalytics Inc. http://www.thermoanalytics.com/support/publications/batterymodelsdoc.html.
[20] V. Srinivasan, J. Weidner, J. Newman, Hysteresis during cycling of nickel hydroxide active material, J. Electrochem. Soc. 148 (9) (2001) A969–A980.
[21] E. Wan, A. Nelson, Dual extended Kalman filter methods, in: S. Haykin (Ed.), Kalman Filtering and Neural Networks, Wiley/Interscience, New York, 2001, pp. 123–174.